18 March 2002

ELSEVIER

Chemical Physics Letters 354 (2002) 403–408

CHEMICAL PHYSICS LETTERS

www.elsevier.com/locate/cplett

Nanofacet-resolved CO oxidation kinetics on alumina-supported Pd particles

J. Hoffmann [a], S. Schauermann [a], J. Hartmann [a], V.P. Zhdanov [b,c], B. Kasemo [b], J. Libuda [a,*], H.-J. Freund [a]

[a] *Fritz-Haber-Institut der Max-Planck-Gesellschaft, Abt. Chemische Physik, Faradayweg 4-6, D-14195 Berlin, Germany*
[b] *Department of Applied Physics, Chalmers University of Technology, S-412 96 Göteborg, Sweden*
[c] *Boreskov Institute of Catalysis, Russian Academy of Sciences, Novosibirsk 630090, Russia*

Received 17 January 2002

Abstract

Employing a multi-molecular-beam approach, we have measured the angular distribution of CO_2 molecules formed during CO oxidation under steady-state conditions on well oriented and shaped nm-sized Pd crystallites grown on an ordered alumina film. The experiment is combined with kinetic Monte Carlo simulations based on a realistic structural model. The results obtained allow us (i) to differentiate between local reaction rates on the particle nanofacets and (ii) to conclude that oxygen diffusion on and between the (1 1 1) facets is rapid compared to reaction.

Heterogeneous catalysis is an interdisciplinary field of natural sciences with immense practical impact, as it forms the mainstay of chemical industry and environmental technologies [1]. In academic studies, catalysis is usually explored on single-crystal surfaces. In practice, however, catalytic reactions often occur on very small (~10 nm) crystalline metal particles deposited on the pore walls of a more or less inactive support. The underlying microscopic reaction kinetics on such catalysts are still poorly understood, because of the limited experimental information on surface structures and processes on nm catalyst particles under reaction conditions. Experimentally, this problem can be addressed by using modern techniques aiming at the preparation of supported model catalysts, which consist of well controlled arrays of metal particles deposited on a planar oxide surface. Systems of this type have recently been used in studies of the global reaction kinetics [2–5]. Unfortunately, there are essentially no experimental tools, which may provide the corresponding site-resolved kinetic information under in situ conditions. Potentially, fast scanning tunneling microscopy [6] and/or photoemission electron microscopy [7] may be applied to model catalysts, however, these methods remain limited with respect to the accessible range of experimental conditions and the kinetic information supplied.

* Corresponding author. Fax: +49-30-84134101.
E-mail address: libuda@fhi-berlin.mpg.de (J. Libuda).

0009-2614/02/$ - see front matter
PII: S0009-2614(02)00151-3

In this Letter, we suggest a new approach to this problem, which is based on measurements of the angular distribution of the reaction products desorbing from ordered and oriented nanoparticles, performed by angular-resolved mass spectrometry. This detection technique in combination with a multi-molecular-beam approach allows us to control individually the impingement and reaction rates on different crystallite facets. In this case, the reactant angular distribution can provide a signature of the reactive sites, at which it has been formed, and accordingly makes it possible to clarify intimate details of elementary reaction steps.

All the experiments were performed at the Fritz-Haber-Institute (Berlin) in a special ultra-high-vacuum apparatus [8] making it possible to cross up to three molecular beams on the sample surface (Fig. 1). The reaction products are observed with a rotatable doubly differentially pumped quadrupole mass spectrometer (QMS) in an angular resolved mode or by a non-differentially pumped QMS in an angular integrated mode. Under reaction conditions, the adsorbate coverages are controlled via in situ IR reflection absorption spectroscopy.

Here, we explore the CO–O_2 reaction on Pd particles (Fig. 2a) [9] grown on a well-ordered alumina film prepared by oxidizing a NiAl(1 1 0) single crystal [10]. The mean particle diameter and height are about 5.5 and 1.7 nm, respectively. On average, the particles contain about 2700 atoms with 20% of them at the surface. About 20% of the surface atoms are located in the top facet, the rest belong to the side facets. Both the top and the side facets have (1 1 1) geometry (the fraction of (1 0 0) facets is small). Under reaction conditions applied in this work, the particles remain stable for at least two days after pre-stabilizing the sample by oxygen exposure at elevated temperatures.

In our experiments, the incidence angle of the O_2 beam, which is generated from a supersonic expansion, is 35° with respect to the surface normal (Fig. 1b). From the beam and particle geometry, it follows that for all Pd crystallites the top facets and the side facets facing the oxygen beam have similar inclination angles with respect to the O_2 beam. Thus, they are exposed to similar direct O_2 fluxes. The side facets on the opposite side of particles are shaded from direct collisions with O_2 molecules. The second reactant, ^{13}CO, is supplied in a symmetric manner by superimposing two CO beams (the use of beam sources instead of CO exposure via the background pressure and isotopically labeled CO drastically reduces the noise level in the measurements).

Under steady-state conditions, the global reaction rate as a function of the fraction of CO in the total impingement rate, $x_{CO} = F_{CO}/(F_{CO} + F_{O_2})$ (F_{CO} and F_{O_2} are the CO and O_2 fluxes), typically shows a maximum, dividing two characteristic regimes (Fig. 3a) [11]. The catalyst is either primarily

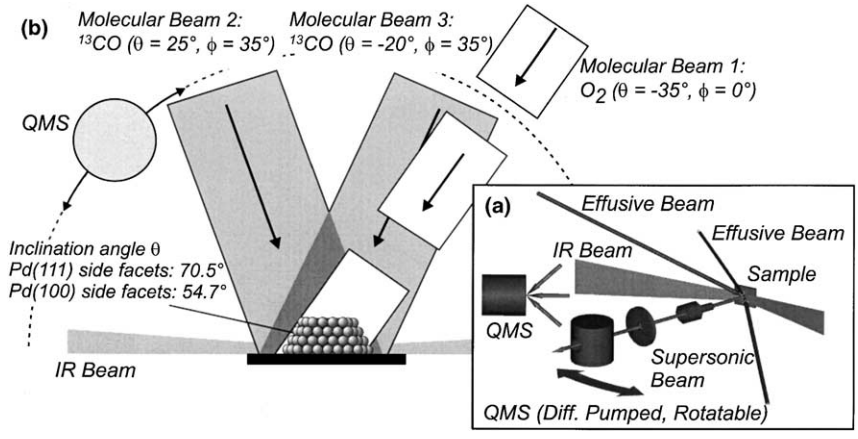

Fig. 1. Schematic representation of (a) the molecular-beam experiment and (b) the experimental setup used in this work.

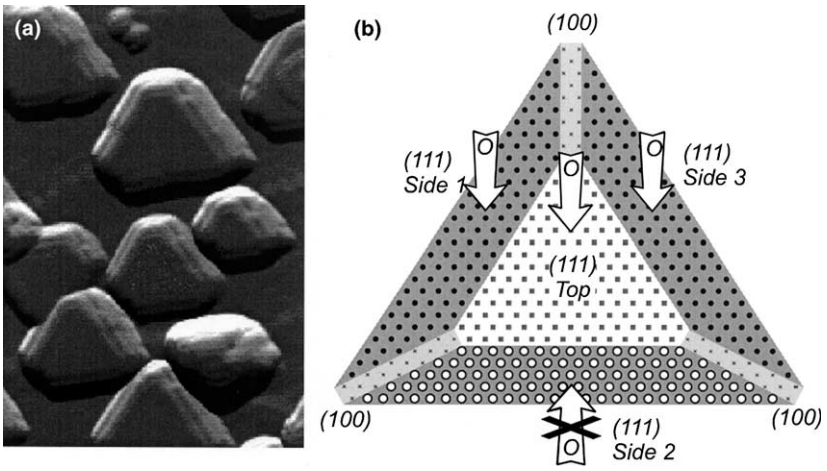

Fig. 2. (a) STM image (35 nm × 25 nm) of the alumina-supported Pd particles and (b) the corresponding lattice model used in the simulations (the arrows indicate the oxygen flux).

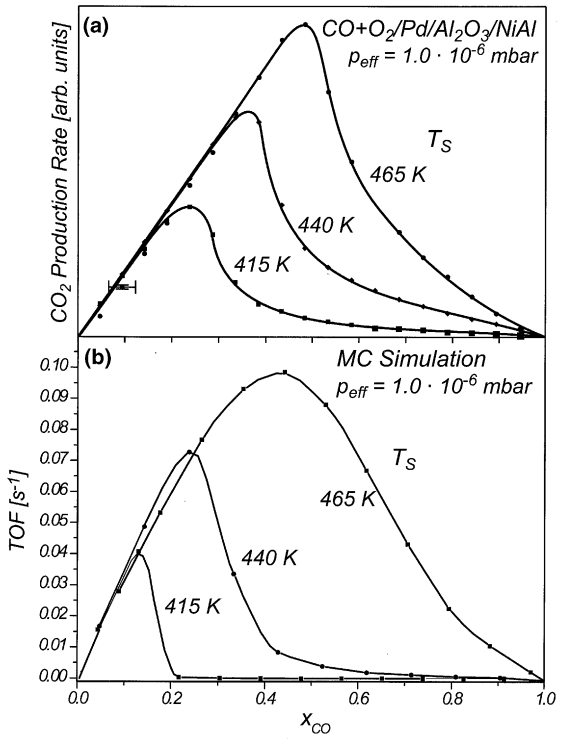

Fig. 3. Angular-integrated steady-state reaction rates as a function of the CO fraction in the total reactant flux at different sample temperatures: (a) experimental data (for details, see [11]); (b) results of the simulations with $p_{\mathrm{dif}}^{\mathrm{O}} = 1$ and $p_{\mathrm{cyc}} = 0.01$ (each data point is obtained by averaging over 5000 MCS).

covered by adsorbed O at O_2 excess or by CO at CO excess (the left and right sides of Fig. 3, respectively). In the angular resolved experiments (see e.g. Fig. 4a for 465 K), we probe the CO_2 angular distributions corresponding to both reaction regimes. It is observed that (i) the CO_2 distribution is broader than a cosine distribution and (ii) the asymmetry of the distribution is small under all conditions and close to the detection limit of the experiment.

(i) To interpret the CO_2 angular distribution, we take into account that adsorption of this species on the Pt-group metals is extremely weak, leading to desorption on a very short time scale after formation [12]. The potential energy surface governing the CO_2 angular distribution depends on the local surrounding of adsorbates. For CO oxidation on Pd(1 1 1), the distribution has been found to be close to the cosine law at low coverage [11a], while at higher coverage, lateral adsorbate interactions result in a CO_2 flux strongly peaked along the surface normal [11b]. We interpret the observation of the broadened angular distribution to be due to CO_2 formation on the side facets of the Pd particles and desorption along the corresponding facet normals.

(ii) The weak asymmetry observed for the angular distributions indicates that despite the fact that there is no O_2 supply on the shaded side of the

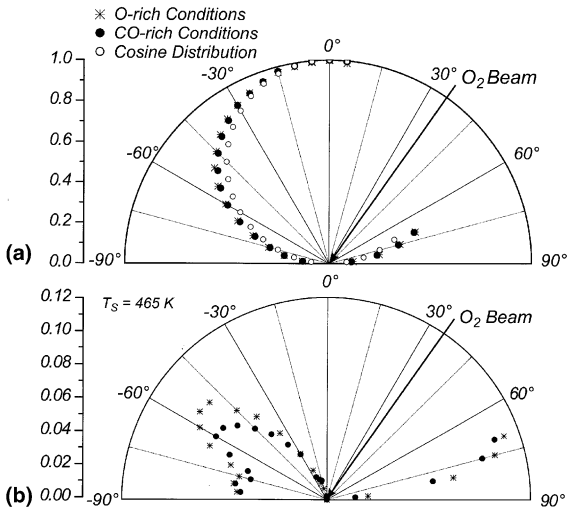

Fig. 4. (a) Angular distributions of CO_2 molecules desorbing from the supported Pd crystallites at $T_s = 465$ K under O_2- and CO-rich reaction conditions (the corresponding total CO beam intensities are 3.2 and 6.4×10^{14} cm^{-2} s^{-1}; the O_2 beam intensity is approximately equal to 4×10^{14} cm^{-2} s^{-1} in both cases). At polar angles between 10 and 65°, no data are available due to shadowing of the supersonic beam by the rotatable mass spectrometer. (b) Polar plot of the difference between the CO_2 angular distribution and the cosine distribution. (To reduce drifts, the displayed data represent an average over both scanning directions. The results have been corrected for the angular-dependent acceptance function of the detector as described in [8].)

Pd crystallites, adsorbed oxygen is distributed homogeneously over the full particle on the time scale of reaction. Partly, this effect may be connected with diffuse scattering of O_2 and/or diffusion of O_2 and CO_2 via weakly bound precursor states on the particles as well as on the support. A possible contribution of these factors is however expected to be minor (the average length of diffusion in the precursor state is e.g. appreciably smaller than the crystallite size). Moreover, steering effects due to an attractive molecule–surface interaction potential might have to be taken into account in a quantitative analysis of the exact flux impinging on the facets [13]. However, we expect steering not to be a dominating effect in the present case, as the long range interaction potential is relatively weak and the size of the particles is rather large on the length scale of the attractive forces. Thus, in a qualitative discussion, we may conclude that the nearly complete equilibration of the chemisorbed oxygen requires rapid diffusion of this species on the reaction time scale.

Taking into account that quantitative information on oxygen diffusion on Pd single crystal surfaces was lacking so far, we have scrutinized the role of this process in the CO oxidation on Pd particles by using Monte Carlo (MC) simulations (see [14] for applications of this technique to nm chemistry). The physics implemented into our model is as follows: (i) Our earlier mean-field analysis [11] indicates that the apparent Arrhenius parameters for the CO_2-formation step on the supported particle system used here are close to those on the (1 1 1) face. Thus, we assume that CO oxidation is dominated by the (1 1 1) facets. Specifically, the Pd particle is represented by a truncated triangle, constructed from a hexagonal lattice (Fig. 2b). Catalytically, all sites are considered to be equivalent. (ii) The nearest-neighbor (nn) O–O lateral interaction is well known to be strongly repulsive. To mimic this effect, we prohibit O adsorption in nn sites (consequently, O_2 adsorption is considered to initially produce O adatoms in next-nearest-neighbor (nnn) vacant sites) and introduce a weak nnn O–O repulsion (8 kJ/mol). As a result, the model predicts the experimentally observed formation of the $p(2 \times 2)-O$ structure at saturation coverage of $\simeq 0.25$ ML [15]. (iii) At low coverage, CO adsorbs mainly in three-fold hollow sites, but may occupy bridge and on-top sites at higher coverages (see e.g. [16] and references therein). For simplicity, we take into account only one type of adsorption sites and allow CO adsorption only if not more than three CO molecules are located in nn sites in order to reproduce the experimental saturation coverages. (iv) CO strongly inhibits O_2 adsorption (see e.g. [12]). To mimic this effect, we prohibit O_2 adsorption if at least one of the sites for adsorption has more than two nn CO molecules (this rule is however not applied to O diffusion). (v) For the CO and O_2 adsorption rate constants, we use the experimental values (in particular, $k_{ad} \equiv k_{ad}^{CO} + k_{ad}^{O_2} = 0.5$ s^{-1} at approximately 10^{-6} mbar total pressure of the three beams). For CO desorption and CO + O reaction, the Arrhenius parameters are $E_{des} = 136$ kJ/mol, $\nu_{des} = 10^{15}$ s^{-1}, $E_{rea} =$

60 kJ/mol, and $\nu_{rea} = 8 \times 10^7$ s^{-1} [11]. At 465 K, the corresponding rate constants are $k_{des} = 0.5$ s^{-1} and $k_{rea} = 15$ s^{-1}, respectively. For CO diffusion, one has $E_{dif}^{CO} = 17$ kJ/mol and $D_\circ = 2.2 \times 10^{-3}$ cm^2 s^{-1} [17], and accordingly at 465 K the CO jump rate is about 10^{10} s^{-1}. Thus, CO diffusion is very rapid compared to all other steps. To characterize the ratio of the rates of O diffusion and catalytic cycle to that of CO diffusion, we employ the dimensionless parameters p_{dif}^{O} and p_{cyc}, respectively. To save computational time, a CO jump rate is used, which is only 100 times higher than the reaction rate, i.e., $p_{cyc} = 0.01$. This rate was found to be sufficient in order to reproduce a homogeneous distribution of CO under all conditions.

With the specifications above, our MC algorithm is as follows:

(1) A random number ρ ($\rho \leqslant 1$) is generated. If $\rho < p_{cyc}$, an adsorption–reaction trial is realized (item (2)). For $\rho > p_{cyc}$, an adsorbate-diffusion trial is performed (item (3)).

(2) An adsorption–reaction attempt contains several steps. (i) An adsorption site on the catalyst particle is chosen at random. (ii) A new random number ρ' is generated. (iii) If the site selected is vacant, CO or O_2 adsorption events are realized as described above provided that $\rho' < p_{CO}$ and $p_{CO} < \rho' < p_{CO} + p_{O_2}$, where $p_{CO} = k_{ad}^{CO}/(k_{des} + k_{rea})$ and $p_{O_2} = k_{ad}^{O_2}/(k_{des} + k_{rea})$ are the normalized adsorption probabilities. (iv) If the site selected is occupied by CO, a CO desorption or reaction event is realized for $\rho' < p_{des}$ and $\rho' > p_{des}$, where $p_{des} = k_{des}/(k_{des} + k_{rea})$. For the CO reaction, one nn site is chosen at random, and the trial is fulfilled if the latter site is occupied by O. (v) If the site is occupied by O, the trial ends (note that the reaction is executed in the CO branch (item (iv))).

(3) For adsorbate diffusion, an adsorption site is chosen at random. If the site is vacant, the trial ends. Otherwise, a CO or O particle located on this site tries to diffuse. In particular, an adjacent site is randomly selected, and if the latter site is vacant and located on the particle lattice, and there are no spatial constraints (as described above), CO jumps to the destination site with unit probability. Jumps of O are executed with the probability p_{dif} combined with the standard Metropolis rule in order to take into account the O–O lateral interactions.

In order to relate the MC time to the number of reaction attempts, we define one MC step as N_s trials of a adsorption–reaction event (N_s is the number of adsorption sites). This means that MC time is calculated by multiplying the total number of trials by p_{cyc}/N_s. With this definition, the MC and real time are interconnected as $t_{MC} = (k_{des} + k_{rea})t$.

First, we have calculated the angular-integrated reaction kinetics with O_2 adsorption on all facets (Fig. 3b). The agreement between experiment and simulation is found to be good at all rates of O diffusion (cf. e.g. Fig. 3a,b). Minor deviations remain with respect to the temperature dependence, which are related to the coverage dependencies of the activation barriers (see e.g. [11]). It is of interest to note that in agreement with our experimental observations no hysteresis in the CO_2 formation rate is found with the present set of kinetic parameters (this effect is, however, possible for other sets of parameters [18]).

To simulate the angular-resolved experiments, we switch off the oxygen adsorption on one of the side facets (Fig. 2b). As expected, the reaction rate on this facet (Fig. 5a) and the occupation of the shaded facet by oxygen (Fig. 5b–e) increase with increasing O diffusion rate in this case. Under oxygen-rich conditions, the rate on this facet becomes indistinguishable from that on the non-shaded facets for $p_{dif}^{O} \simeq 1$ (this value corresponds to $k_{dif}^{O} \simeq 1500$ s^{-1}, or to $E_{dif}^{O} = 85$ kJ/mol provided that the pre-exponential factor is 'normal', $D_\circ = 10^{-3}$ cm^2 s^{-1}). At the same diffusion rate and under CO-rich conditions, approximately 80% of the maximum rate is obtained on the shaded facet. The difference arises as a consequence of the changes on the oxygen residence time, which depends on the steady-state coverages. The above given value for the diffusion barrier should be considered as an experimental upper limit. So far, no other quantitative experimental data are available for oxygen diffusion on Pd single crystal surfaces. The value is consistent with recent theoretical investigations which provide an estimate of 54 kJ/mol for the diffusion barrier on Pd(1 1 1) [19]. However, it cannot be excluded that on the nanoparticles in addition to the regular diffusion

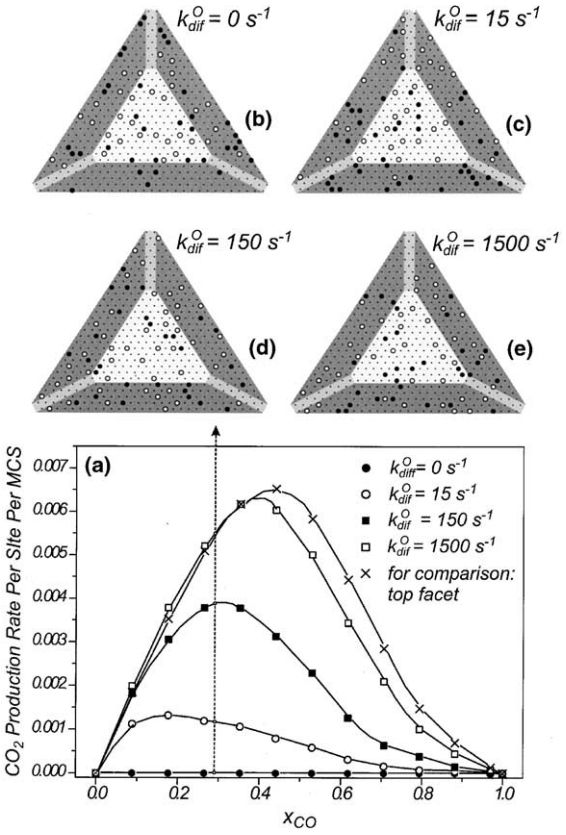

Fig. 5. (a) Steady-state reaction rate on the shaded facet at different rates of oxygen diffusion for $T_s = 465$ K. For comparison, the reaction rate on the top (central) facet at high O and CO mobility is added. (b)–(e) Snapshots of the lattice under steady-state reaction conditions with no oxygen adsorption on the shaded side (bottom) facet for $x_{CO} = 0.29$ and different rates of oxygen surface diffusion. Oxygen atoms and CO molecules are indicated by open and filled circles, respectively.

barriers the contribution of steps and edges is considerable.

In summary, we have shown that a combination of multiple molecular-beam techniques and angular-resolved mass spectroscopy makes it possible to directly monitor reaction rates on the various facets of the supported nanocrystallites and to obtain novel information on the rates of elementary reaction steps. In particular, we have derived that under reaction conditions an upper limit for the activation energy of oxygen diffusion on Pd crystallites is about 85 kJ/mol.

Acknowledgements

The project has been funded by the Deutsche Forschungsgemeinschaft and the Max-Planck Society. The authors thank M. Bäumer and M. Heemeier for the STM data used in this work.

References

[1] J.M. Thomas, W.J. Thomas, Principles and Practice of Heterogeneous Catalysis, VCH, Weinheim, 1997.
[2] C.R. Henry, Surf. Sci. Rep. 31 (1998) 231.
[3] H.-J. Freund, M. Bäumer, H. Kuhlenbeck, Surf. Sci. Rep. 31 (1998) 231.
[4] J. Zhu, G.A. Somorjai, Nano Lett. 1 (2001) 8.
[5] S. Johansson, L. Österlund, B. Kasemo, J. Catal. 201 (2001) 275.
[6] J. Wintterlin, Adv. Catal. 45 (2000) 131;
J. Wintterlin et al., Science 278 (1997) 1931.
[7] W. Huang, R. Zhai, X. Bao, Langmuir 17 (2001) 3629.
[8] J. Libuda et al., Rev. Sci. Instrum. 71 (2000) 4395.
[9] M. Bäumer, H.-J. Freund, Prog. Surf. Sci. 61 (1999) 127.
[10] R.M. Jaeger et al., Surf. Sci. 259 (1991) 235;
J. Libuda et al., Surf. Sci. 318 (1994) 61.
[11] (a) J. Libuda et al., J. Chem. Phys. 114 (2001) 4669;
(b) J. Hoffmann et al., J. Catal. 204 (2001) 378.
[12] (a) T. Engel, G. Ertl, Chem. Phys. Lett. 54 (1978) 95;
(b) T. Matsushima, H. Asada, J. Chem. Phys. 85 (1986) 1658.
[13] S. Van Dijken, L.C. Jorritsma, B. Poelsema, Phys. Rev. Lett. 82 (1999) 4038.
[14] V.P. Zhdanov, B. Kasemo, Surf. Sci. Rep. 39 (2000) 25.
[15] H. Conrad et al., Surf. Sci. 65 (1977) 245.
[16] T. Gießel et al., Surf. Sci. 406 (1998) 90.
[17] M. Snabl et al., Surf. Sci. 385 (1997) L1016.
[18] V.P. Zhdanov, B. Kasemo, Surf. Sci. 496 (2002) 251.
[19] K. Honkala, K. Laasonen, J. Chem. Phys. 115 (2001) 2297.